

Observation of Scaling Violations in Scaled Momentum Distributions at HERA

ZEUS Collaboration

Abstract

Charged particle production has been measured in deep inelastic scattering (DIS) events over a large range of x and Q^2 using the ZEUS detector. The evolution of the scaled momentum, x_p , with Q^2 , in the range 10 to 1280 GeV², has been investigated in the current fragmentation region of the Breit frame. The results show clear evidence, in a single experiment, for scaling violations in scaled momenta as a function of Q^2 .

The ZEUS Collaboration

J. Breitweg, M. Derrick, D. Krakauer, S. Magill, D. Mikunas, B. Musgrave, J. Repond, R. Stanek, R.L. Talaga, R. Yoshida, H. Zhang

Argonne National Laboratory, Argonne, IL, USA ^p

M.C.K. Mattingly

Andrews University, Berrien Springs, MI, USA

F. Anselmo, P. Antonioli, G. Bari, M. Basile, L. Bellagamba, D. Boscherini, A. Bruni, G. Bruni, G. Cara Romeo, G. Castellini¹, L. Cifarelli², F. Cindolo, A. Contin, M. Corradi, S. De Pasquale, I. Gialas³, P. Giusti, G. Iacobucci, G. Laurenti, G. Levi, A. Margotti, T. Massam, R. Nania, F. Palmonari, A. Pesci, A. Polini, F. Ricci, G. Sartorelli, Y. Zamora Garcia⁴, A. Zichichi

University and INFN Bologna, Bologna, Italy ^f

C. Amelung, A. Bornheim, I. Brock, K. Coböken, J. Crittenden, R. Deffner, M. Eckert, M. Grothe, H. Hartmann, K. Heinloth, L. Heinz, E. Hilger, H.-P. Jakob, U.F. Katz, R. Kerger, E. Paul, M. Pfeiffer, Ch. Rembser⁵, J. Stamm, R. Wedemeyer⁶, H. Wieber

Physikalisches Institut der Universität Bonn, Bonn, Germany ^c

D.S. Bailey, S. Campbell-Robson, W.N. Cottingham, B. Foster, R. Hall-Wilton, M.E. Hayes, G.P. Heath, H.F. Heath, J.D. McFall, D. Piccioni, D.G. Roff, R.J. Tapper

H.H. Wills Physics Laboratory, University of Bristol, Bristol, U.K. ^o

M. Arneodo⁷, R. Ayad, M. Capua, A. Garfagnini, L. Iannotti, M. Schioppa, G. Susinno

Calabria University, Physics Dept.and INFN, Cosenza, Italy ^f

J.Y. Kim, J.H. Lee, I.T. Lim, M.Y. Pac⁸

Chonnam National University, Kwangju, Korea ^h

A. Caldwell⁹, N. Cartiglia, Z. Jing, W. Liu, B. Mellado, J.A. Parsons, S. Ritz¹⁰, S. Sampson, F. Sciulli, P.B. Straub, Q. Zhu

Columbia University, Nevis Labs., Irvington on Hudson, N.Y., USA ^q

P. Borzemski, J. Chwastowski, A. Eskreys, J. Figiel, K. Klimek, M.B. Przybycień, L. Zawiejski

Inst. of Nuclear Physics, Cracow, Poland ^j

L. Adamczyk¹¹, B. Bednarek, M. Bukowy, K. Jeleń, D. Kisielewska, T. Kowalski,

M. Przybycień, E. Rulikowska-Zarębska, L. Suszycki, J. Zając

Faculty of Physics and Nuclear Techniques, Academy of Mining and Metallurgy, Cracow, Poland ^j

Z. Duliński, A. Kotański

Jagellonian Univ., Dept. of Physics, Cracow, Poland ^k

G. Abbiendi¹², L.A.T. Bauerdick, U. Behrens, H. Beier, J.K. Bienlein, G. Cases¹³, O. Deppe, K. Desler, G. Drews, U. Fricke, D.J. Gilkinson, C. Glasman, P. Göttlicher, T. Haas, W. Hain, D. Hasell, K.F. Johnson¹⁴, M. Kasemann, W. Koch, U. Kötzt, H. Kowalski, J. Labs, L. Lindemann, B. Löhr, M. Löwe¹⁵, O. Mańczak, J. Milewski, T. Monteiro¹⁶, J.S.T. Ng¹⁷, D. Notz, K. Ohrenberg¹⁸, I.H. Park¹⁹, A. Pellegrino, F. Pelucchi, K. Piotrkowski, M. Roco²⁰, M. Rohde, J. Roldán, J.J. Ryan, A.A. Savin, U. Schneekloth, F. Selonke, B. Surrow, E. Tassi, T. Voß²¹, D. Westphal, G. Wolf, U. Wollmer²², C. Youngman, A.F. Żarnecki, W. Zeuner
Deutsches Elektronen-Synchrotron DESY, Hamburg, Germany

B.D. Burow, H.J. Grabosch, A. Meyer, S. Schlenstedt
DESY-IfH Zeuthen, Zeuthen, Germany

G. Barbagli, E. Gallo, P. Pelfer
University and INFN, Florence, Italy^f

G. Maccarrone, L. Votano
INFN, Laboratori Nazionali di Frascati, Frascati, Italy^f

A. Bamberger, S. Eisenhardt, P. Markun, T. Trefzger²³, S. Wölfle
Fakultät für Physik der Universität Freiburg i.Br., Freiburg i.Br., Germany^c

J.T. Bromley, N.H. Brook, P.J. Bussey, A.T. Doyle, N. Macdonald, D.H. Saxon, L.E. Sinclair, E. Strickland, R. Waugh
Dept. of Physics and Astronomy, University of Glasgow, Glasgow, U.K.^o

I. Bohnet, N. Gendner, U. Holm, A. Meyer-Larsen, H. Salehi, K. Wick
Hamburg University, I. Institute of Exp. Physics, Hamburg, Germany^c

L.K. Gladilin²⁴, D. Horstmann, D. Kçira, R. Klanner, E. Lohrmann, G. Poelz, W. Schott²⁵, F. Zetsche
Hamburg University, II. Institute of Exp. Physics, Hamburg, Germany^c

T.C. Bacon, I. Butterworth, J.E. Cole, G. Howell, B.H.Y. Hung, L. Lamberti²⁶, K.R. Long, D.B. Miller, N. Pavel, A. Prinias²⁷, J.K. Sedgbeer, D. Sideris
Imperial College London, High Energy Nuclear Physics Group, London, U.K.^o

U. Mallik, S.M. Wang, J.T. Wu
University of Iowa, Physics and Astronomy Dept., Iowa City, USA^p

P. Cloth, D. Filges
Forschungszentrum Jülich, Institut für Kernphysik, Jülich, Germany

J.I. Fleck⁵, T. Ishii, M. Kuze, I. Suzuki²⁸, K. Tokushuku, S. Yamada, K. Yamauchi, Y. Yamazaki²⁹
Institute of Particle and Nuclear Studies, KEK, Tsukuba, Japan^g

S.J. Hong, S.B. Lee, S.W. Nam³⁰, S.K. Park
Korea University, Seoul, Korea^h

F. Barreiro, J.P. Fernández, G. García, R. Graciani, J.M. Hernández, L. Hervás⁵, L. Labarga, M. Martínez, J. del Peso, J. Puga, J. Terrón³¹, J.F. de Trocóniz
Univer. Autónoma Madrid, Depto de Física Teórica, Madrid, Spainⁿ

F. Corriveau, D.S. Hanna, J. Hartmann, L.W. Hung, W.N. Murray, A. Ochs, M. Riveline, D.G. Stairs, M. St-Laurent, R. Ullmann
McGill University, Dept. of Physics, Montréal, Québec, Canada^{a, b}

T. Tsurugai
Meiji Gakuin University, Faculty of General Education, Yokohama, Japan

V. Bashkirov, B.A. Dolgoshein, A. Stifutkin
Moscow Engineering Physics Institute, Moscow, Russia^l

G.L. Bashindzhagyan, P.F. Ermolov, Yu.A. Golubkov, L.A. Khein, N.A. Korotkova, I.A. Korzhavina, V.A. Kuzmin, O.Yu. Lukina, A.S. Proskuryakov, L.M. Shcheglova³², A.N. Solomin³², S.A. Zotkin
Moscow State University, Institute of Nuclear Physics, Moscow, Russia^m

C. Bokel, M. Botje, N. Brümmer, F. Chlebana²⁰, J. Engelen, E. Koffeman, P. Kooijman, A. van Sighem, H. Tiecke, N. Tuning, W. Verkerke, J. Vossebeld, M. Vreeswijk⁵, L. Wiggers, E. de Wolf
*NIKHEF and University of Amsterdam, Amsterdam, Netherlands*ⁱ

D. Acosta, B. Bylsma, L.S. Durkin, J. Gilmore, C.M. Ginsburg, C.L. Kim, T.Y. Ling, P. Nylander, T.A. Romanowski³³
Ohio State University, Physics Department, Columbus, Ohio, USA^p

H.E. Blaikley, R.J. Cashmore, A.M. Cooper-Sarkar, R.C.E. Devenish, J.K. Edmonds, J. Große-Knetter³⁴, N. Harnew, C. Nath, V.A. Noyes³⁵, A. Quadt, O. Ruske, J.R. Tickner²⁷, H. Uijterwaal, R. Walczak, D.S. Waters
Department of Physics, University of Oxford, Oxford, U.K.^o

A. Bertolin, R. Brugnera, R. Carlin, F. Dal Corso, U. Dosselli, S. Limentani, M. Morandin, M. Posocco, L. Stanco, R. Stroili, C. Voci
Dipartimento di Fisica dell'Università and INFN, Padova, Italy^f

J. Bulmahn, B.Y. Oh, J.R. Okrasinski, W.S. Toothacker, J.J. Whitmore
Pennsylvania State University, Dept. of Physics, University Park, PA, USA^q

Y. Iga
Polytechnic University, Sagamihara, Japan^g

G. D'Agostini, G. Marini, A. Nigro, M. Raso
Dipartimento di Fisica, Univ. 'La Sapienza' and INFN, Rome, Italy^f

J.C. Hart, N.A. McCubbin, T.P. Shah
Rutherford Appleton Laboratory, Chilton, Didcot, Oxon, U.K.^o

D. Epperson, C. Heusch, J.T. Rahn, H.F.-W. Sadrozinski, A. Seiden, R. Wichmann, D.C. Williams
University of California, Santa Cruz, CA, USA^p

O. Schwarzer, A.H. Walenta
Fachbereich Physik der Universität-Gesamthochschule Siegen, Germany^c

H. Abramowicz³⁶, G. Briskin, S. Dagan³⁶, S. Kananov³⁶, A. Levy³⁶
*Raymond and Beverly Sackler Faculty of Exact Sciences, School of Physics, Tel-Aviv University,
Tel-Aviv, Israel*^e

T. Abe, T. Fusayasu, M. Inuzuka, K. Nagano, K. Umemori, T. Yamashita
Department of Physics, University of Tokyo, Tokyo, Japan^g

R. Hamatsu, T. Hirose, K. Homma³⁷, S. Kitamura³⁸, T. Matsushita
Tokyo Metropolitan University, Dept. of Physics, Tokyo, Japan^g

R. Cirio, M. Costa, M.I. Ferrero, S. Maselli, V. Monaco, C. Peroni, M.C. Petrucci, M. Ruspa,
R. Sacchi, A. Solano, A. Staiano
Università di Torino, Dipartimento di Fisica Sperimentale and INFN, Torino, Italy^f

M. Dardo
II Faculty of Sciences, Torino University and INFN - Alessandria, Italy^f

D.C. Bailey, C.-P. Fagerstroem, R. Galea, G.F. Hartner, K.K. Joo, G.M. Levman, J.F. Martin,
R.S. Orr, S. Polenz, A. Sabetfakhri, D. Simmons, R.J. Teuscher⁵
University of Toronto, Dept. of Physics, Toronto, Ont., Canada^a

J.M. Butterworth, C.D. Catterall, T.W. Jones, J.B. Lane, R.L. Saunders, M.R. Sutton, M. Wing
University College London, Physics and Astronomy Dept., London, U.K.^o

J. Ciborowski, G. Grzelak³⁹, M. Kasprzak, K. Muchorowski⁴⁰, R.J. Nowak, J.M. Pawlak,
R. Pawlak, T. Tymieniecka, A.K. Wróblewski, J.A. Zakrzewski
Warsaw University, Institute of Experimental Physics, Warsaw, Poland^j

M. Adamus
Institute for Nuclear Studies, Warsaw, Poland^j

C. Coldewey, Y. Eisenberg³⁶, D. Hochman, U. Karshon³⁶
Weizmann Institute, Department of Particle Physics, Rehovot, Israel^d

W.F. Badgett, D. Chapin, R. Cross, S. Dasu, C. Foudas, R.J. Loveless, S. Mattingly, D.D. Reeder,
W.H. Smith, A. Vaiciulis, M. Wodarczyk
University of Wisconsin, Dept. of Physics, Madison, WI, USA^p

S. Bhadra, W.R. Frisken, M. Khakzad, W.B. Schmidke
York University, Dept. of Physics, North York, Ont., Canada^a

¹ also at IROE Florence, Italy
² now at Univ. of Salerno and INFN Napoli, Italy
³ now at Univ. of Crete, Greece
⁴ supported by Worldlab, Lausanne, Switzerland
⁵ now at CERN
⁶ retired
⁷ also at University of Torino and Alexander von Humboldt Fellow at DESY
⁸ now at Dongshin University, Naju, Korea
⁹ also at DESY
¹⁰ Alfred P. Sloan Foundation Fellow
¹¹ supported by the Polish State Committee for Scientific Research, grant No. 2P03B14912
¹² supported by an EC fellowship number ERBFMBICT 950172
¹³ now at SAP A.G., Walldorf
¹⁴ visitor from Florida State University
¹⁵ now at ALCATEL Mobile Communication GmbH, Stuttgart
¹⁶ supported by European Community Program PRAXIS XXI
¹⁷ now at DESY-Group FDET
¹⁸ now at DESY Computer Center
¹⁹ visitor from Kyungpook National University, Taegu, Korea, partially supported by DESY
²⁰ now at Fermi National Accelerator Laboratory (FNAL), Batavia, IL, USA
²¹ now at NORCOM Infosystems, Hamburg
²² now at Oxford University, supported by DAAD fellowship HSP II-AUFE III
²³ now at ATLAS Collaboration, Univ. of Munich
²⁴ on leave from MSU, supported by the GIF, contract I-0444-176.07/95
²⁵ now a self-employed consultant
²⁶ supported by an EC fellowship
²⁷ PPARC Post-doctoral Fellow
²⁸ now at Osaka Univ., Osaka, Japan
²⁹ supported by JSPS Postdoctoral Fellowships for Research Abroad
³⁰ now at Wayne State University, Detroit
³¹ partially supported by Comunidad Autonoma Madrid
³² partially supported by the Foundation for German-Russian Collaboration DFG-RFBR
(grant no. 436 RUS 113/248/3 and no. 436 RUS 113/248/2)
³³ now at Department of Energy, Washington
³⁴ supported by the Feodor Lynen Program of the Alexander von Humboldt foundation
³⁵ Glasstone Fellow
³⁶ supported by a MINERVA Fellowship
³⁷ now at ICEPP, Univ. of Tokyo, Tokyo, Japan
³⁸ present address: Tokyo Metropolitan College of Allied Medical Sciences, Tokyo 116, Japan
³⁹ supported by the Polish State Committee for Scientific Research, grant No. 2P03B09308
⁴⁰ supported by the Polish State Committee for Scientific Research, grant No. 2P03B09208

- ^a supported by the Natural Sciences and Engineering Research Council of Canada (NSERC)
- ^b supported by the FCAR of Québec, Canada
- ^c supported by the German Federal Ministry for Education and Science, Research and Technology (BMBF), under contract numbers 057BN19P, 057FR19P, 057HH19P, 057HH29P, 057SI75I
- ^d supported by the MINERVA Gesellschaft für Forschung GmbH, the German Israeli Foundation, and the U.S.-Israel Binational Science Foundation
- ^e supported by the German Israeli Foundation, and by the Israel Science Foundation
- ^f supported by the Italian National Institute for Nuclear Physics (INFN)
- ^g supported by the Japanese Ministry of Education, Science and Culture (the Monbusho) and its grants for Scientific Research
- ^h supported by the Korean Ministry of Education and Korea Science and Engineering Foundation
- ⁱ supported by the Netherlands Foundation for Research on Matter (FOM)
- ^j supported by the Polish State Committee for Scientific Research, grant No. 115/E-343/SPUB/P03/002/97, 2P03B10512, 2P03B10612, 2P03B14212, 2P03B10412
- ^k supported by the Polish State Committee for Scientific Research (grant No. 2P03B08308) and Foundation for Polish-German Collaboration
- ^l partially supported by the German Federal Ministry for Education and Science, Research and Technology (BMBF)
- ^m supported by the Fund for Fundamental Research of Russian Ministry for Science and Education and by the German Federal Ministry for Education and Science, Research and Technology (BMBF)
- ⁿ supported by the Spanish Ministry of Education and Science through funds provided by CICYT
- ^o supported by the Particle Physics and Astronomy Research Council
- ^p supported by the US Department of Energy
- ^q supported by the US National Science Foundation

1 Introduction

The observation of scaling violations in structure functions [1] measured in neutral current, deep inelastic scattering (DIS) helped to establish Quantum Chromodynamics (QCD) as the theory of strong interactions and has led to measurements of the strong coupling constant, α_s . Similar scaling violations are predicted in the fragmentation functions, which represent the probability for a parton to fragment into a particular hadron carrying a fraction of the parton's energy. Fragmentation functions incorporate the long distance, non-perturbative physics of the hadronization process in which the observed hadrons are formed from final state partons of the hard scattering process and, like structure functions, cannot be calculated in perturbative QCD, but can be evolved from a starting distribution at a defined energy scale. If the fragmentation functions are combined with the cross sections for the inclusive production of each parton type in the given physical process, predictions can be made for scaling violations in the scaled momentum spectra of final state hadrons [2]. These scaling violations allow a measurement of α_s and such studies have been performed at LEP [3, 4] by incorporating lower energy PETRA data.

The event kinematics of DIS are determined by the negative square of the 4-momentum transfer at the positron vertex, $Q^2 \equiv -q^2$, and the Bjorken scaling variable, $x = Q^2/2P \cdot q$, where P is the four-momentum of the proton. In the Quark Parton Model (QPM), the interacting quark from the proton carries the four-momentum xP . The variable y , the fractional energy transfer to the proton in its rest frame, is related to x and Q^2 by $y \simeq Q^2/xs$, where \sqrt{s} is the positron-proton centre of mass energy. A natural frame in which to study the dynamics of the hadronic final state in DIS is the Breit frame [5, 6], which has been used in previous studies of QCD effects [7, 8, 9] at HERA. In this frame the exchanged virtual boson is purely space-like with 3-momentum $\vec{q} = (0, 0, -Q)$, the incident quark carries momentum $Q/2$ in the positive Z -direction, and the outgoing struck quark carries $Q/2$ in the negative Z -direction. A final state particle has momentum p^B in this frame, and is assigned to the current region if p_Z^B is negative, and to the target frame if p_Z^B is positive. The advantage of this frame lies in the maximal separation of the outgoing parton from radiation associated with the incoming parton and the proton remnant, thus providing the optimal environment for the study of its fragmentation.

In this analysis the inclusive charged particle distributions of the scaled momenta, x_p , in the current region of the Breit frame are measured; x_p is the momentum of a track measured in the Breit frame, p^B , scaled by $Q/2$, the maximum possible momentum (ignoring effects due to the intrinsic k_T of the quark within the proton).

The scaled momentum distributions are studied as a function of Q and x , in the range $6 \times 10^{-4} < x < 5 \times 10^{-2}$ and $10 < Q^2 < 1280 \text{ GeV}^2$. Thus the evolution of fragmentation functions can be observed within a single experiment over a wide range of Q . A similar analysis has recently been performed by the H1 collaboration [10].

2 Experimental Setup

The data presented here were taken in 1994 at the positron-proton collider HERA using the ZEUS detector. During this period HERA operated with positrons of energy $E_e = 27.5$ GeV and protons with energy 820 GeV. The data of this analysis correspond to a luminosity of 2.50 ± 0.04 pb⁻¹. A detailed description of the ZEUS detector can be found in [11, 12]; we present here a brief description of the components most relevant to the present analysis.

Throughout this paper we use the standard ZEUS right-handed coordinate system, in which $X = Y = Z = 0$ is the nominal interaction point, the positive Z -axis points in the direction of the proton beam (referred to as the forward direction) and the X -axis is horizontal, pointing towards the centre of HERA.

The tracking system consists of a vertex detector (VXD) [13] and a central tracking chamber (CTD) [14] enclosed in a 1.43 T solenoidal magnetic field. Immediately surrounding the beampipe is the VXD which consists of 120 radial cells, each with 12 sense wires. The CTD, which encloses the VXD, is a drift chamber consisting of 72 cylindrical layers, arranged in 9 superlayers. Superlayers with wires parallel to the beam axis alternate with those inclined at a small angle to give a stereo view. The single hit efficiency of the CTD is greater than 95% and the measured resolution in transverse momentum for tracks with hits in all the superlayers is $\sigma_{p_T}/p_T = 0.005p_T \oplus 0.016$ (p_T in GeV).

Outside the solenoid is the uranium-scintillator calorimeter (CAL) [15], which is divided into three parts: forward, barrel and rear covering the polar regions 2.6° to 36.7° , 36.7° to 129.1° and 129.1° to 176.2° , respectively. The CAL covers 99.7% of the solid angle, with holes of 20×20 cm² in the centres of the forward and rear calorimeters to accommodate the HERA beam pipe. Each of the calorimeter parts is subdivided into towers which are segmented longitudinally into electromagnetic (EMC) and hadronic (HAC) sections. These sections are further subdivided into cells each of which is read out by two photomultipliers. From test beam data, energy resolutions of $\sigma_E/E = 0.18/\sqrt{E}$ for electrons and $\sigma_E/E = 0.35/\sqrt{E}$ for hadrons (E in GeV) have been obtained.

The small angle rear tracking detector (SRTD) [16], which is attached to the front face of the rear calorimeter, measures the impact point of charged particles at small angles with respect to the positron beam direction.

The luminosity is measured by means of the Bethe-Heitler process $ep \rightarrow e\gamma p$, by detecting the photon in a calorimeter [17] positioned at $Z = -107$ m which has an energy resolution of $\sigma_E/E = 0.18/\sqrt{E(\text{GeV})}$ under test beam conditions. The luminosity calorimeter is also used to tag photons from initial state radiation in DIS events.

3 Kinematic Reconstruction

The ZEUS detector is almost hermetic, allowing the kinematic variables x and Q^2 to be reconstructed in a variety of ways using combinations of positron and hadronic system energies and

angles. Variables calculated only from the measurements of the energy, E'_e , and angle, θ_e , of the scattered positrons are denoted with the subscript e , whilst those calculated from the hadronic system measurements, with the Jacquet Blondel method [18], are denoted by the subscript JB . Variables calculated by these approaches are only used in the event selection. In the double angle method [19], denoted by DA , the kinematic variables are determined using θ_e and the angle γ_H (which is the direction of the struck quark in QPM), defined from the hadronic final state:

$$\cos \gamma_H = \frac{(\sum_i p_X)^2 + (\sum_i p_Y)^2 - (\sum_i (E - p_Z))^2}{(\sum_i p_X)^2 + (\sum_i p_Y)^2 + (\sum_i (E - p_Z))^2},$$

where the sums run over all CAL cells i , excluding those assigned to the scattered positron, and $\vec{p} = (p_X, p_Y, p_Z)$ is the 3-momentum assigned to a cell of energy E . The cell angles are calculated from the geometric centre of the cell and the vertex position of the event. This angle is then combined with the measured angle of the scattered positron to calculate x and Q^2 . The two angles can also be used to recalculate the energy of the scattered positron:

$$E'_{DA} = \frac{2E_e \sin \gamma_H}{\sin \gamma_H + \sin \theta_e - \sin(\gamma_H + \theta_e)}.$$

The DA method was used throughout this analysis for the calculation of the boosts and the kinematic variables because it is less sensitive to systematic uncertainties in the energy measurement than the other methods discussed above.

An additional method of measuring y and Q^2 (the PT method [20]) was used as a systematic check of the kinematic reconstruction to determine the binning of the data and the boost vector. This method uses a more sophisticated combination of the information from the measurements of both the hadronic system and the positron.

In order to boost to the Breit frame it is necessary to calculate the velocity of the Breit frame with respect to the laboratory frame, which is given by $\vec{\beta} = (\vec{q} + 2x\vec{P})/(q_0 + 2xP_0)$ where (q_0, \vec{q}) and (P_0, \vec{P}) are the 4-momenta of the exchanged photon and the incident proton beam respectively. The event is then rotated so that the virtual photon is along the negative Z -axis. The Breit frame boost vector was reconstructed using E'_{DA} and the polar and azimuthal angles measured from the impact point of the scattered e^+ on the calorimeter or SRTD. The 4-momentum vectors of the charged particles were boosted to the Breit frame, assuming the pion mass to determine the particle's energy, and were assigned to the current region if $p_Z^B < 0$.

4 Event Reconstruction and Selection

The triggering and online event selections were identical to those used for the measurement of the structure function F_2 [20].

To reduce the effects of noise due to the uranium radioactivity on the calorimetric measurements all EMC (HAC) cells with an energy deposit of less than 60 (110) MeV were discarded from the analysis. For cells with isolated energy deposits this cut was increased to 100 (150) MeV.

The track finding algorithm starts with hits in the outer axial superlayers of the CTD. As the trajectory is followed inwards towards the beam axis, hits from inner superlayers are added to the track. The momentum vector is determined in a 5-parameter helix fit. The reconstructed tracks used in this analysis are associated with the primary event vertex and have $p_T > 150$ MeV and $|\eta| < 1.75$, where η is the pseudorapidity given by $-\ln(\tan(\theta/2))$ with θ being the polar angle of the measured track with respect to the proton direction. This is a region of high CTD acceptance where the detector response and systematics are best understood.

Further selection criteria were applied both to ensure accurate reconstruction of the kinematic variables and to increase the purity of the sample by eliminating background from photoproduction processes. These cuts were:

- $E'_e \geq 10$ GeV, to achieve a high purity sample of DIS events;
- $Q_{DA}^2 \geq 10$ GeV²;
- $y_e \leq 0.95$, to reduce the photoproduction background;
- $y_{JB} \geq 0.04$, to give sufficient accuracy for DA reconstruction;
- $35 \leq \delta = \sum_i (E - p_Z) \leq 60$ GeV summed over all calorimeter cells, to remove photoproduction events and events with large radiative corrections.
- $|X| > 16$ cm or $|Y| > 16$ cm, where X and Y are the impact position of the positron on the CAL as determined using the SRTD to avoid the region directly adjacent to the rear beam pipe.
- $-40 < Z_{\text{vertex}} < 50$ cm, to reduce background events from non ep collisions.

In total, 68066 events satisfy the above cuts and are reconstructed in the (x, Q^2) bins (as calculated by the DA method) that are listed in Table 1. The sizes of the bins in x and Q^2 were chosen to have good statistics in each bin and to limit the migrations between bins [7].

5 QCD Models and Event Simulation

Monte Carlo event simulation is used to correct for acceptance and resolution effects. The detector simulation is based on the GEANT 3.13 [21] program and incorporates our best knowledge of the apparatus.

To calculate the acceptance, neutral current DIS events were generated, via the DJANGO program [22], using HERACLES [23] which incorporates first order electroweak corrections. The QCD cascade was modelled with the colour-dipole model including the boson-gluon fusion process, using the ARIADNE 4.08 [24] program. In this model coherence effects are implicitly included in the formalism of the parton cascade. This program uses the Lund string fragmentation model [25] for the hadronisation phase, as implemented in JETSET 7.3 [26]. Two Monte Carlo samples were generated, 1.6 pb^{-1} with $Q^2 > 3 \text{ GeV}^2$ and 2.6 pb^{-1} with $Q^2 > 6 \text{ GeV}^2$,

using the MRSA [27] parameterisation of the parton distribution functions. Another approach to modelling the parton cascade is included in the LEPTO(6.5.1) [28] program, which incorporates the LO matrix element matched to parton showers (MEPS). This program also uses the Lund string fragmentation model and was used for the generator level calculations used in comparisons to our data.

For the studies of the systematics, two additional samples of events were generated (1.2 pb^{-1} with $Q^2 > 4 \text{ GeV}^2$ and 3.2 pb^{-1} with $Q^2 > 100 \text{ GeV}^2$) using the HERWIG 5.8c Monte Carlo [29], where no electroweak radiative corrections were applied. In HERWIG, coherence effects in the QCD cascades are included by angular ordering of successive parton emissions and a clustering model is used for the hadronisation [30, 31]. For this sample the parameterisation of the parton distribution functions was the MRSA' set [32]. The MRSA and MRSA' parameterisations have both been shown to describe reasonably well the HERA measurements of the proton structure function F_2 in the (x, Q^2) range of this analysis [33, 34].

6 Correction Procedure

Monte Carlo event generator studies were used to determine the mean charged particle acceptance in the current region as a function of (x, Q^2) . The chosen analysis intervals in (x, Q^2) correspond to regions of high acceptance, 74 to 96%, in the current region of the Breit frame.

x_{DA} range	Q_{DA}^2 (GeV^2) range	No. of events
$6.0 - 12.0 \times 10^{-4}$	10 - 20	13898
	20 - 40	8484
	40 - 80	5093
$1.2 - 2.4 \times 10^{-3}$	10 - 20	11899
	20 - 40	9399
	40 - 80	9493
	80 - 160	5031
$2.4 - 10.0 \times 10^{-3}$	160 - 320	1369
	160 - 320	2131
	320 - 640	916
	640 - 1280	353

Table 1: The (x, Q^2) analysis bins showing the the numbers of accepted events in the (x, Q^2) bins as reconstructed by the DA method.

Uncertainty in the reconstruction of the boost vector, $\vec{\beta}$, was found to be the most significant factor on the resolution of x_p and it leads to the choice of variable bin width in x_p . Migration of tracks from the current region to the target region was typically $\simeq 6$ to 8% of the tracks generated in the current region. Migrations into the current region from the target fragmentation region are typically less than 5% of the tracks assigned to the current region for

$Q^2 > 320 \text{ GeV}^2$. For $10 < Q^2 < 320 \text{ GeV}^2$ these migrations are generally of the order of 10 to 15%. At $Q^2 < 40 \text{ GeV}^2$ and low values of y this assignment can be as high as $\simeq 25\%$, since in the low y region the hadronic activity is low and the measurement of γ_H becomes distorted by noise in the calorimeter leading to a worse x resolution and hence an uncertainty in $\vec{\beta}$.

The correction procedure is based on the detailed Monte Carlo simulation of the ZEUS detector with the event generators described in the previous section. Since the ARIADNE model gives the best overall description of our observed energy flow [35] it is used for the standard corrections to the distributions.

The data are corrected for trigger and event selection cuts; event migration between (x, Q^2) intervals; QED radiative effects; track reconstruction efficiency; track selection cuts in p_T and η ; track migration between the current and target regions; and for the products of Λ and K_S^0 decays which are assigned to the primary vertex.

Correction factors were obtained from the Monte Carlo simulation by comparing the generated distributions, without Λ and K_S^0 decay products, with the reconstructed distributions after the detector and trigger simulations followed by the same reconstruction, selection and analysis as the real data. The correction factors, $F(x_p)$, were calculated for each x_p bin with the formula:

$$F(x_p) = \frac{1}{N_{\text{gen}}} \left(\frac{dn}{dx_p} \right)_{\text{gen}} \bigg/ \frac{1}{N_{\text{obs}}} \left(\frac{dn}{dx_p} \right)_{\text{obs}}$$

where N_{gen} (N_{obs}) is the number of generated (observed) Monte Carlo events in each (x, Q^2) interval and n is the number of charged particles (tracks) in the current region in the corresponding (x, Q^2) interval. The correction factors are typically between 1.0 and 1.3, except in the lowest x_p bin ($0.02 < x_p < 0.05$) of the two lowest Q^2 bins where they are about 1.5.

7 Results

The inclusive charged particle distributions, $1/\sigma_{\text{tot}}d\sigma/dx_p$ where σ_{tot} is the DIS cross section in the chosen (x, Q^2) bin, are shown in figure 1. In the low (x, Q^2) regions these distributions peak at $x_p \approx 0.2$ with a broad tail out to 1. As Q^2 increases the data fall off more sharply from the minimum x_p . In the same figure the ARIADNE Monte Carlo generator predictions are also shown, which are in good agreement with the data. The increasingly steep fall-off towards higher values of x_p as Q^2 increases corresponds to the production of more particles with a smaller fractional momentum, and is indicative of scaling violation in the fragmentation function. These scaling violations can be seen more clearly if the data are plotted in bins of fixed x_p as a function of Q^2 . Figure 2 shows the charged particle distributions with statistical errors combined in quadrature with the systematic errors which will be discussed below. For $Q^2 > 80 \text{ GeV}^2$ the distributions rise with Q^2 at low x_p and fall-off at high x_p and high Q^2 . By measuring the amount of scaling violation one can ultimately measure the amount of parton radiation and thus determine α_s . Below $Q^2 = 80 \text{ GeV}^2$ the fall-off is due to depopulation of the current region discussed later.

7.1 Systematic Studies

The systematic uncertainties in the measurement can be divided into three classes: errors due to event reconstruction and selection; to track reconstruction and selection; and to the Monte Carlo generator used.

- **Event Reconstruction and Selection**

The event selection procedure was checked by altering the y_e, y_{JB} and δ cuts: the resulting shifts of the corrected distributions were small, with all points moving systematically in the same direction at the ± 1 to 3% level. By removing the noise suppression, described in section 4, a systematic shift at the ± 1 to 3% level is produced. Using the boost calculated from the PT method produced a larger shift: for $Q^2 < 160 \text{ GeV}^2$ the systematic shift is +10 to 15% at large x_p , whilst +2 to 5% at small x_p ; for $Q^2 \geq 160 \text{ GeV}^2$ the systematic shift is constant with x_p at the +2 to 5% level.

- **Track Reconstruction and Selection**

The major systematic on the track reconstruction was obtained considering all reconstructed tracks as opposed to only those assigned to the primary vertex. This produced a typical shift of 2 to 6% with no systematic dependence on the value of x_p , except in the bin $0.02 < x_p < 0.05$ at low Q^2 and x where the systematic shift was up to +15%. Tightening the tracking cuts on $|\eta|$ and p_T particularly affected those (x, Q^2) bins where the track acceptance is strongly dependent on the negative η cut. The general trend is for the cross section to be shifted to higher values. The bins most affected have an average shift of up to 5%, whilst in general the shift is $\lesssim 1\%$.

- **Monte Carlo Generator**

Using a different Monte Carlo generator (HERWIG rather than ARIADNE) led to distributions which were systematically lower by about 10% in the range of $0 \leq x_p \leq 0.3$. In the range $x_p > 0.5$, the HERWIG corrected distributions were systematically higher (lower) by 5 to 10 % for $Q^2 < 40 \text{ GeV}^2$ ($Q^2 > 100 \text{ GeV}^2$). In the range $0.3 \leq x_p \leq 0.4$ the two generators gave results that were in good agreement.

All positive (negative) systematic shifts in each of the x_p bins were combined in quadrature to give an estimate of the overall positive (negative) systematic uncertainty on the measurement. These systematic shifts do not affect the observation of scaling violations.

7.2 Discussion

Fragmentation in DIS of a quark carrying momentum $Q/2$ in the Breit frame may be compared to fragmentation in e^+e^- annihilation of the produced q and \bar{q} , each carrying momentum $\sqrt{s_{e^+e^-}}/2$. In figure 2 the ZEUS data are compared at $Q^2 = s_{e^+e^-}$ to e^+e^- data [36], divided by two to account for the production of both a q and \bar{q} . The e^+e^- data have also been corrected by $\simeq 8\%$ for the decay products of Λ and K_S^0 , using the JETSET 7.3 Monte Carlo tuned to DELPHI data. In the Q^2 range shown there is good agreement between the current region of

the Breit frame in DIS and the e^+e^- experiments. When our data are compared with the lower energy SPEAR [37] data ($\sqrt{s} = 5.2, 6.5$ GeV, not shown) discrepancies begin to show up. They can be explained in terms of the kinematic depopulation of the current region described in the next paragraph.

The turnover observed in the ZEUS data at low x_p and low Q^2 , figure 2, can be attributed to processes not present in e^+e^- (eg scattering off a sea quark and/or boson gluon fusion) depopulating the current region [8]. This is best illustrated when discussing the production of a pair of partons in DIS with a large invariant mass, \hat{s} [6]. When $Q^2 \gg \hat{s}$, the radiation is emitted in the direction of the struck quark in the QPM. However, at low Q^2 and low x , \hat{s} is likely to be bigger than Q^2 and the radiation will be emitted in the direction opposite to the QPM direction and will therefore not be in the current region as defined in section 1. In particular, the boson-gluon fusion diagram, which dominates at low- x , provides a significant cross section for large mass radiation [38], thus producing this depopulation.

In figure 3 the data are compared to two leading-log Monte Carlo predictions which are implemented within the Lund fragmentation framework. Our data are well described by the ARIADNE generator, colour dipole model (CDM), over the full range of Q^2 . This is not true for the LEPTO, matrix element+parton showers (MEPS), model. In particular LEPTO overestimate the data at low x_p and there is a greater Q^2 dependence than that suggested by the data. A feature of both Monte Carlo models is a trend that, at fixed Q^2 , the charged particle distribution increases with x . Such a trend is also observed in the data, see fig 2. No tuning of the Monte Carlo parameters has been performed to improve the agreement with the data.

Our results can be compared to the next-to-leading order (NLO) QCD calculations, as implemented in CYCLOPS [39], of the charged particle inclusive distributions in the restricted region $Q^2 > 80$ GeV² and $x_p > 0.1$, where the theoretical uncertainties are small and unaffected by the hadron mass effects which are not included in the fragmentation function [40]. This comparison is shown in figure 4. The NLO calculation combines a full next-to-leading order matrix element with the MRSA' parton densities (with $\Lambda_{\text{QCD}} = 230$ MeV) and NLO fragmentation functions derived by Binnewies et al. from fits to e^+e^- data [41]. The data and the NLO calculations are in good agreement, supporting the idea of universality of quark fragmentation.

8 Conclusions

Charged particle distributions have been studied in the current region of the Breit frame in DIS over a wide range of Q^2 values. These results show clear evidence in a single experiment for scaling violations in scaled momenta as a function of Q^2 . The data are also well described with NLO calculations.

The comparison between e^+e^- data at $Q^2 = s_{e^+e^-}$ and the current region of the Breit frame in DIS for $Q^2 > 80$ GeV² shows also a good agreement. The observed charged particle spectra are consistent with the universality of quark fragmentation in e^+e^- and DIS.

Acknowledgements

We appreciate the contributions to the construction and maintenance of the ZEUS detector by many people who are not listed as authors. We thank the DESY computing staff for providing the data analysis environment. The HERA machine group is especially acknowledged for the outstanding operation of the collider. The strong support and encouragement of the DESY Directorate has been invaluable.

We would like to thank D. Graudenz for valuable discussions and for providing us with the NLO program, CYCLOPS.

References

- [1] R. G. Roberts, ‘The Structure of the Proton’, Cambridge University Press (1990).
- [2] G. Altarelli et al., Nucl. Phys. B160 (1979) 301;
P. Nason and B. R. Webber, Nucl. Phys. B421 (1994) 473.
- [3] ALEPH Collab., D. Buskulic et al., Phys. Lett. B357 (1995) 487.
- [4] DELPHI Collab., P. Abreu et al., Phys. Lett. B311 (1993) 408
DELPHI Collab., P. Abreu et al., CERN-PPE/96-185.
- [5] R. P. Feynman, ‘Photon-Hadron Interactions’, Benjamin, N.Y. (1972).
- [6] K. H. Streng, T. F. Walsh and P. M. Zerwas, Z. Phys. C2 (1979) 237.
- [7] ZEUS Collab., M. Derrick et al., Z. Phys. C67 (1995) 93.
- [8] V. Jamieson, PhD Thesis, University of Glasgow (1994).
- [9] H1 Collab., S Aid et al., Nucl. Phys. B445 (1995) 3;
H1 Collab., C Adloff et al., DESY-97-098, accepted for publication in Phys. Lett. B.
- [10] H1 Collab., C. Adloff et al., DESY 97-108, accepted for publication in Nucl. Phys. B.
- [11] ZEUS Collab., M. Derrick et al., Phys. Lett. B293 (1992) 465;
ZEUS Collab., M. Derrick et al., Z. Phys. C63 (1994) 391.
- [12] ZEUS Collab., The ZEUS Detector, Status Report 1993, DESY 1993.
- [13] C. Alvisi et al., Nucl. Inst. Meth. A305 (1991) 30.
- [14] N. Harnew et al., Nucl. Inst. Meth. A279 (1989) 290;
B. Foster et al., Nucl. Phys. B (Proc. Suppl.) 32 (1993) 181;
B. Foster et al., Nucl. Inst. Meth. A338 (1994) 254.

- [15] M. Derrick et al., Nucl. Inst. Meth. A309 (1991) 77;
A. Andresen et al., Nucl. Inst. Meth. A309 (1991) 101;
A. Bernstein et al., Nucl. Inst. Meth. A336 (1993) 23.
- [16] A. Bamberger et al., DESY 97-157.
- [17] J. Andruszków et al., DESY 92-066 (1992).
- [18] F. Jacquet and A. Blondel, Proceedings of the study for an ep facility for Europe, DESY 79/48 (1979) 391.
- [19] S. Bentvelsen, J. Engelen and P. Kooijman, Proceedings of the 1991 Workshop on Physics at HERA, DESY Vol. 1 (1992) 23.
- [20] ZEUS Collab., M. Derrick et al., Z. Phys. C72 (1996) 399.
- [21] R. Brun et al., GEANT3, CERN DD/EE/84-1 (1987).
- [22] K. Charchuła, G. Schuler and H. Spiesberger, Comp. Phys. Comm. 81 (1994) 381.
- [23] A. Kwiatkowski, H. Spiesberger and H.-J. Möhring, Proceedings of the 1991 Workshop on Physics at HERA, DESY Vol. 3 (1992) 1294.
- [24] L. Lönnblad, ARIADNE version 4.03 program and manual, Comp. Phys. Comm. 71 (1992) 15.
- [25] B. Andersson et al., Phys. Rep. 97 (1983) 31.
- [26] T. Sjöstrand, Comp. Phys. Comm. 82 (1994) 74;
T. Sjöstrand, CERN-TH 7112/93 (revised August 1995).
- [27] A. D. Martin, R. G. Roberts and W. J. Stirling, Phys. Rev. D50 (1994) 6734.
- [28] G. Ingelman, Proceedings of the 1991 Workshop on Physics at HERA, DESY Vol. 3 (1992) 1366.
- [29] G. Marchesini et al., Comp. Phys. Comm. 67 (1992) 465.
- [30] B. Webber, Nucl. Phys. B238 (1984) 492.
- [31] G. Marchesini and B. R. Webber, Nucl. Phys. B310 (1988) 461.
- [32] A. D. Martin, W. J. Stirling and R. G. Roberts, Phys. Lett. B354 (1995) 155.
- [33] ZEUS Collab., M. Derrick et al., Z. Phys. C65 (1995) 379.
- [34] H1 Collab., I. Abt et al., Nucl. Phys. B407 (1993) 515.
- [35] ZEUS Collab., M. Derrick et al., Z. Phys. C59 (1993) 231.

- [36] TASSO Collab., W. Braunschweig et al., *Z. Phys.* C47 (1990) 187;
MARK II Collab., A. Petersen et al., *Phys. Rev.* D37 (1988) 1;
AMY Collab., Y. K. Li et al., *Phys. Rev.* D41 (1990) 2675;
DELPHI Collab., P. Abreu et al., *Phys. Lett.* B311 (1993) 408.
- [37] MARK II Collab., J. F. Patrick et al., *Phys. Rev. Lett.* 49 (1982) 1232.
- [38] ZEUS Collab., M. Derrick et al., *Z. Phys.* C67 (1995) 81.
- [39] D. Graudenz, CERN-TH/96-52;
D. Graudenz, CYCLOPS program and private communication.
- [40] D. Graudenz, PSI-PR/97-20;
- [41] J. Binnewies et al., *Z. Phys.* C65 (1995) 471.

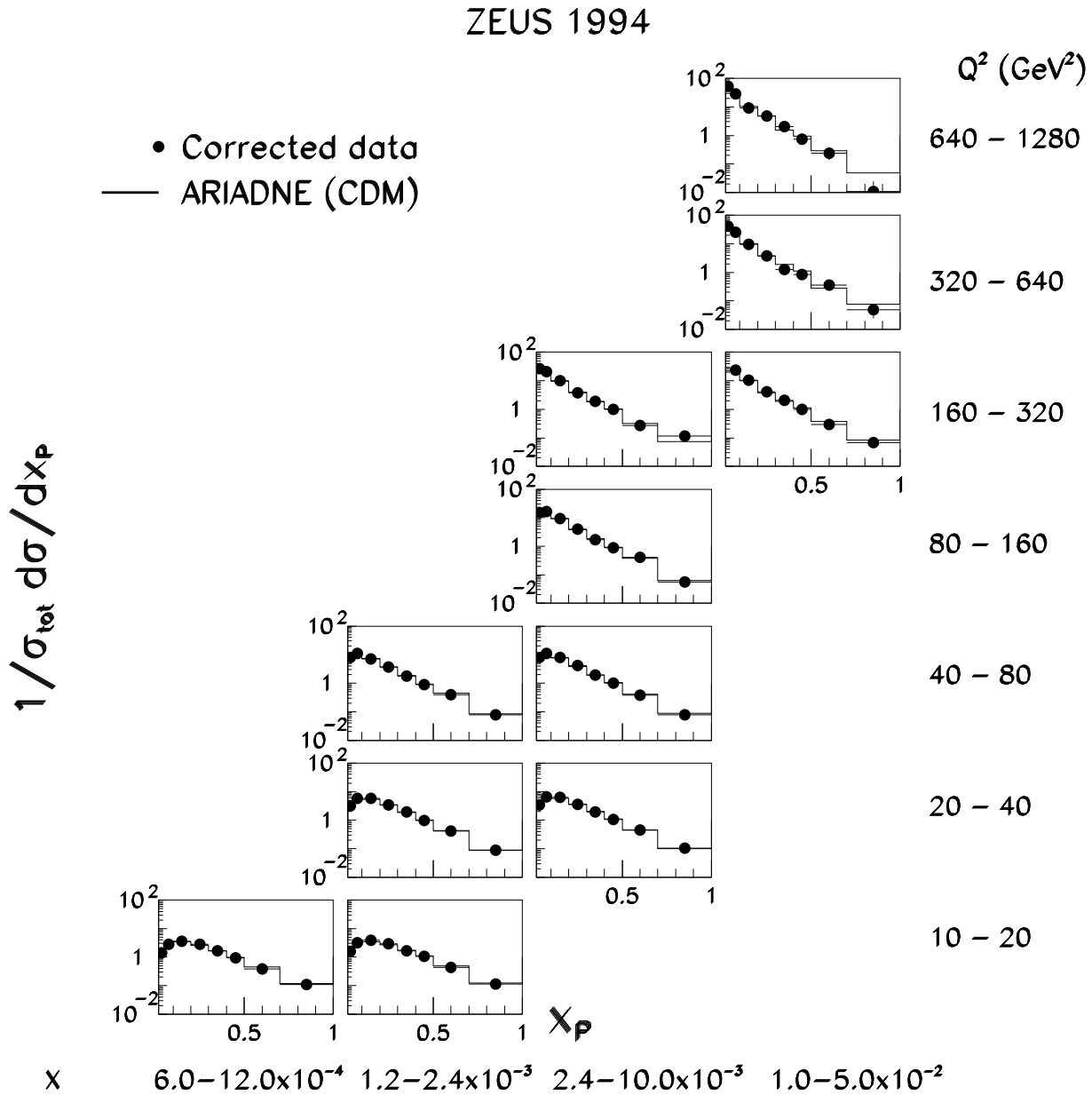


Figure 1: The inclusive charged particle distributions, $1/\sigma_{tot} d\sigma/dx_p$, in the current fragmentation region of the Breit frame compared with the generated distributions from the Monte Carlo (ARIADNE 4.08). The statistical errors are generally within the size of the points.

ZEUS 1994

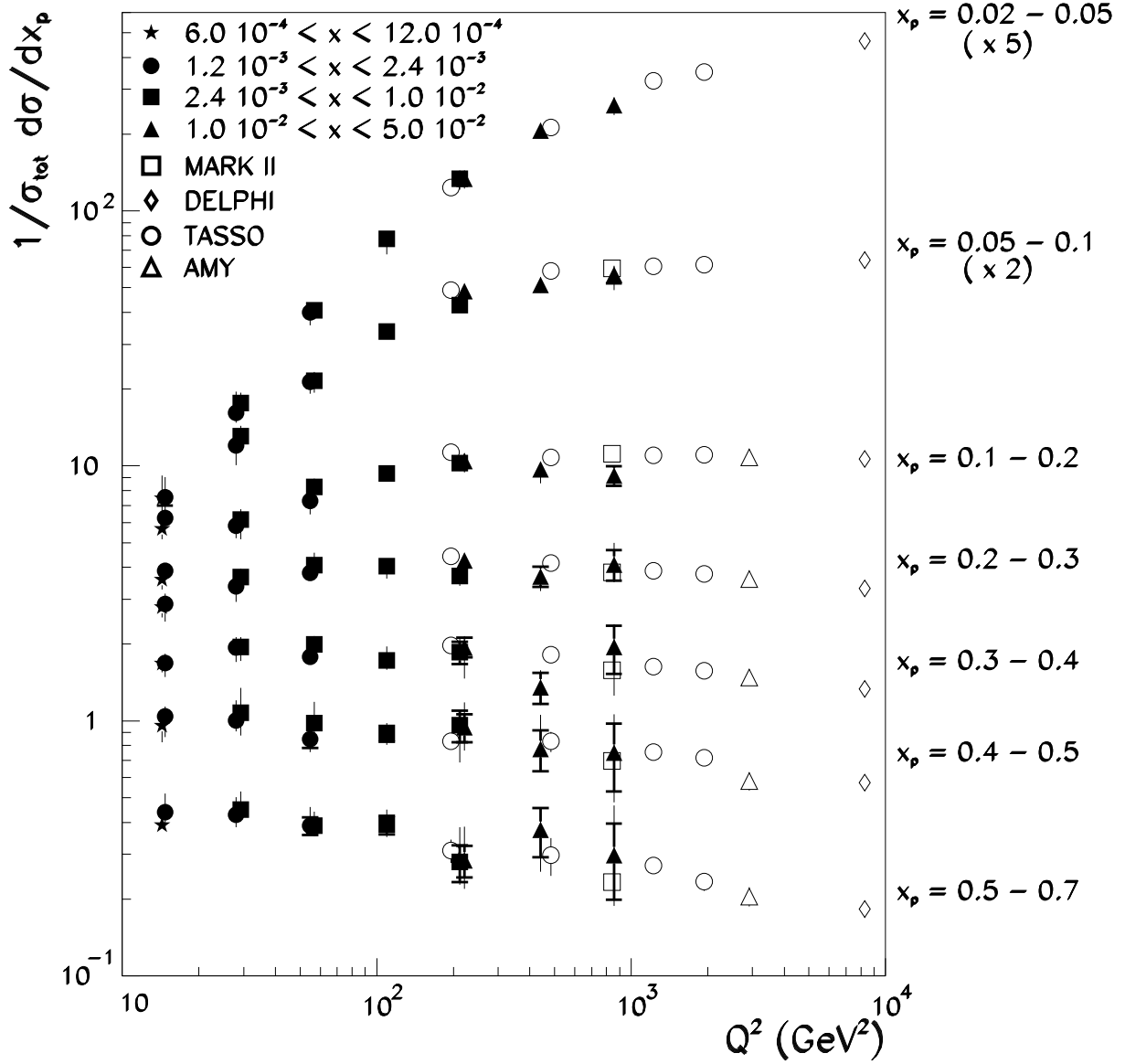


Figure 2: The inclusive charged particle distribution, $1/\sigma_{tot} d\sigma/dx_p$, in the current fragmentation region of the Breit frame. The filled data points are from ZEUS. The full errors are statistical and systematic combined in quadrature. The thick lines denote the statistical error. The open points represent data from e^+e^- experiments divided by two to account for q and \bar{q} production (also corrected for contributions from K_S^0 and Λ .)

ZEUS 1994

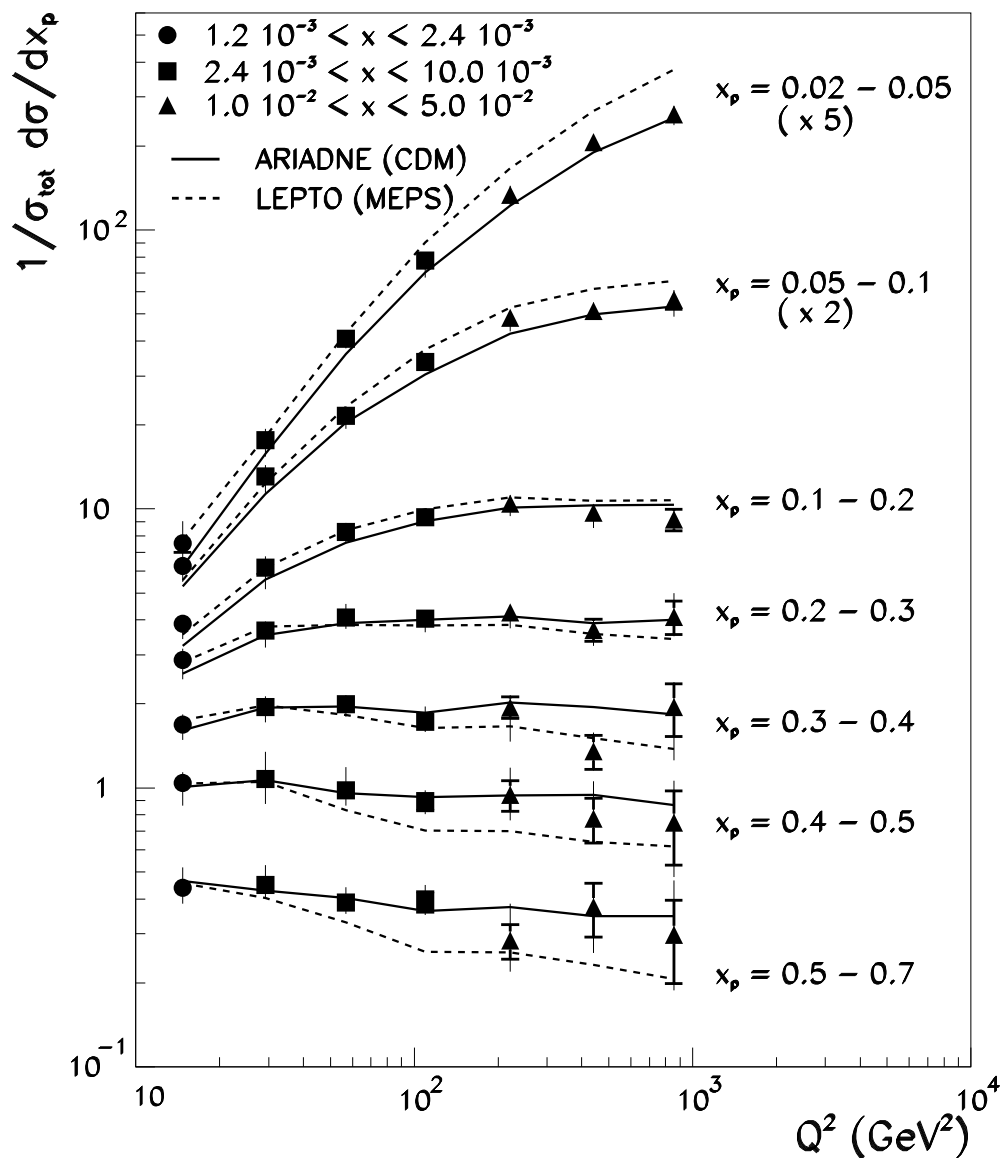


Figure 3: The inclusive charged particle distribution, $1/\sigma_{\text{tot}} d\sigma/dx_p$, in the current fragmentation region of the Breit frame. The data points are from ZEUS. The full errors are statistical and systematic combined in quadrature. The thick lines denote the statistical error. The curves represent leading-log Monte Carlo models: the full line is ARIADNE (CDM) and the dashed line is LEPTO (MEPS). For clarity of presentation, only the higher x bin is shown in each Q^2 interval.

ZEUS 1994

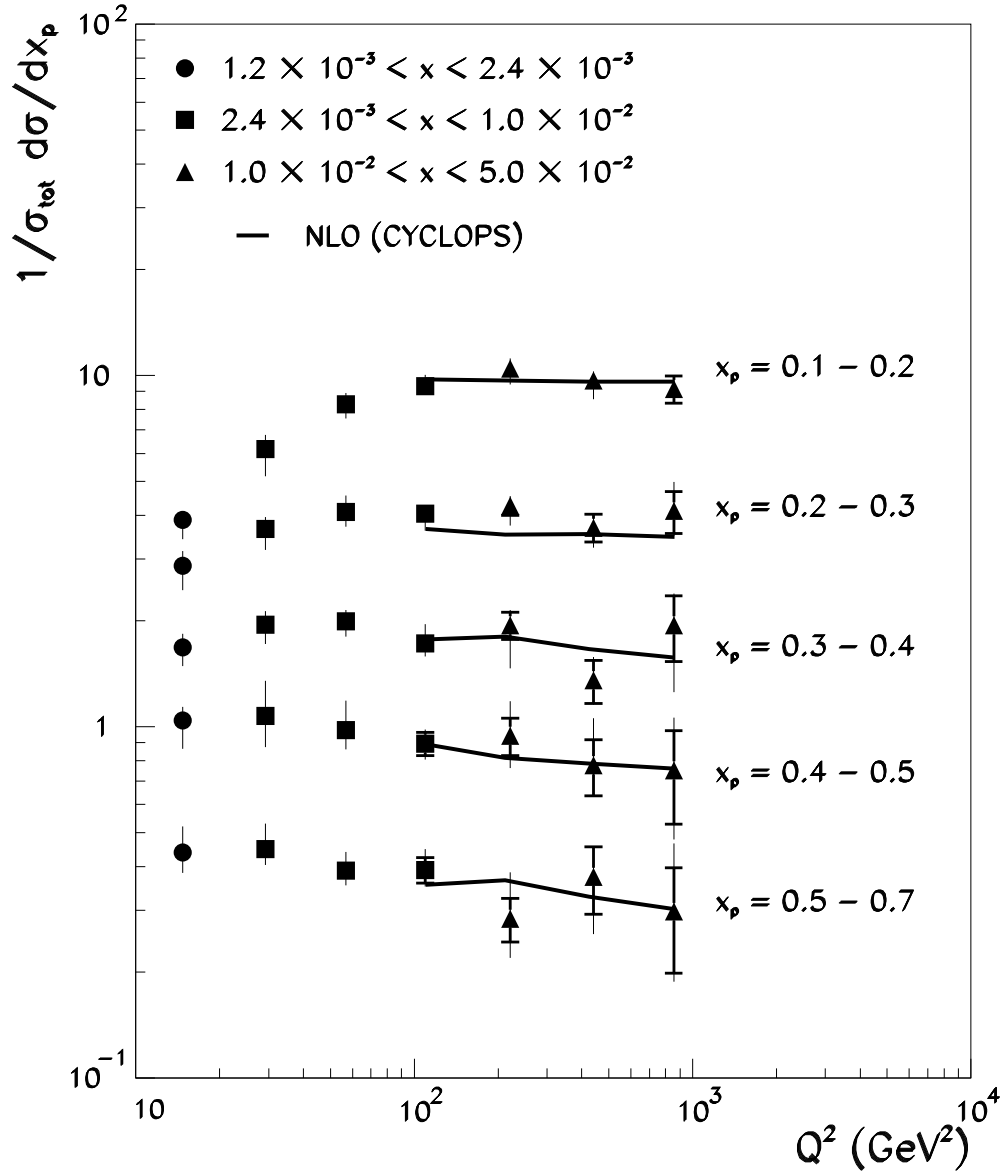


Figure 4: The inclusive charged particle distribution, $1/\sigma_{tot} d\sigma/dx_p$, in the current fragmentation region of the Breit frame compared to the NLO calculation, CYCLOPS [39]. For clarity of presentation, only the higher x bin is shown in each Q^2 interval.